scientific reports

OPEN

Analysis of the forced convection of two-phase Ferro-nanofluid flow in a completely porous microchannel containing rotating cylinders

Hamidreza Aghamiri, Mohammadreza Niknejadi✉ & Davood Toghraie✉

In the present work, the forced convection of nanofluid flow in a microchannel containing rotating cylinders is investigated in different geometries. The heat flux applied to the microchannel wall is 10,000 W m⁻². The effects of Reynolds number, the volume fraction of nanoparticles, and the porosity percentage of the porous medium are investigated on the flow fields, temperature, and heat transfer rate. Reynolds number values vary from Re = 250–1000, non-dimensional rotational velocities 1 and 2, respectively, and volume fraction of nanoparticles 0–2%. The results show that increasing the velocity of rotating cylinders increases the heat transfer; also, increasing the Reynolds number and volume fraction of nanoparticles increases the heat transfer, pressure drop, and $C_{f,ave}$. By comparing the porosity percentages with each other, it is concluded that due to the greater contact of the nanofluid with the porous medium and the creation of higher velocity gradients, the porosity percentage is 45% and the values of are 90% higher than the porosity percentage. Comparing porosity percentages with each other, at porosity percentage 90% is greater than at porosity percentage 45%. On the other hand, increasing the Reynolds number reduces the entropy generation due to heat transfer and increases the entropy generation due to friction. Increasing the volume fraction of nanoparticles increases the entropy generations due to heat transfer and friction.

List of symbols

C_f	Friction factor
C_P	Specific heat $[J\,kg^{-1}\,K^{-1}]$
D_h	Hydraulic diameter $[m]$
$h(x)$	Local heat transfer coefficient $[W\,m^{-2}\,K^{-1}]$
h	Average heat transfer coefficient $[W\,m^{-2}\,K^{-1}]$
k	Thermal conductivity $[W\,m^{-1}\,K^{-1}]$
K	Permeability of porous medium $[m^{-1}]$
L	Characteristic length $[m]$
Δp	Pressure drop $[Pa]$
Re	Reynolds number
S_T'''	Entropy generation due to heat transfer $[W\,m^{-3}\,K^{-1}]$
S_F'''	Entropy generation due to friction $[W\,m^{-3}\,K^{-1}]$
S'''	Total entropy generation $[W\,m^{-3}\,K^{-1}]$
T_b	Bulk temperature $[K]$
T_w	Wall temperature $[K]$
u,v	Velocity vector components $[m\,s^{-1}]$

The growing demand for product downsizing in all industrial sectors has been accompanied by global competition. Much work has been done on single-phase heat transfer in microchannels by Tuckerman and Pease[1] to cool integrated circuits on a very large scale. Today, research in the field of nanofluids has become very extensive.

Department of Mechanical Engineering, Khomeinishahr Branch, Islamic Azad University, Khomeinishahr Khomeinishahr, Iran. ✉email: m.r.niknejadi@iaukhsh.ac.ir; Toghraee@iaukhsh.ac.ir

On the one hand, in connection with increasing the thermal conductivity of fluids and increasing the heat transfer, researchers are pursuing the fabrication of nanofluids with nanoparticles and nanotubes with different nanoparticle sizes. In many industrial applications, porous materials play a very important role in the design and development of processes. Currently, the general model of porous media has a very wide field and it can be divided into different sub-categories depending on the type of application, many of which need to be analyzed. To solve many of the above applications, the physics of heat transfer and flow through porous media must be well understood[2]. Fadaei et al.[3] investigated the forced convection of ferromagnetic nanofluid in a simple channel with a magnetic field and a porous medium. They found that the combined effects of the magnetic field and the porous medium increased the mixing rate and disturbed the thermal boundary layer, which in turn increased the Nu_{ave}. Wang and Li[4] investigated forced convection in a channel containing a porous medium. They found that the use of a porous medium plays an important role in balancing the heat flux of the wall and the heat generated. In addition, with increasing the Darcy number, the Nu_{ave} becomes independent of the porosity property. Li et al.[5] conducted a theoretical study on forced convection in a circular tube assuming an asymmetric inlet temperature. They found that the Nu_{ave} was strongly dependent on the Pecklet number, and the Biot number. They concluded that the proposed solution could be used as a criterion for numerical problems. Xu and Gong[6] investigated the forced convection in a tube, part of which is filled with a porous medium. They found that the porosity gradient had no significant effect on the $C_{f,ave}$ and Nu_{ave} decreased with increasing porosity. Baragh et al.[7] experimentally investigated the convection of fluid in a channel with different porosities. Their results showed that the presence of a porous layer causes more heat transfer of the channel wall to the fluid, which increases the thermal conductivity of the porous material. Li et al.[8] studied convection in a circular tube with a saturated porous medium. They showed that the Pecklet number and the Biot number play an important role in increasing or decreasing heat transfer. Jamal-Abad et al.[9] analyzed heat transfer in a tube filled with a porous medium. Considering the thermal conductivity of the porous medium as a linear function of the radius of the tube and using the Brinkman equation, they found that the Nu_{ave} changes as a linear function of the thermal conductivity of the porous medium. Akyildiz and Siginer[10] proposed a precise solution for the forced convection of a gas flow in a microtube. Heat transfer and flow parameters such as pressure drop (ΔP) were investigated in their research and accurate solutions based on the above parameters were presented, which show an error of less than 5% compared to laboratory results. Zeng et al.[11] performed a laboratory and numerical study of heat transfer in a heat sink. They showed that with the deformation of the blades, the mixing effect increases significantly. Xu et al.[12] numerically investigated the convection in a half-filled tube with a porous medium. Their results showed that the parameters of heat transfer and flow resistance within this type of porous foam are highly dependent on porosity, porosity thickness, and porous pore density. Vijay et al.[13] analyzed the forced convection in open-cell foams. They found that the structure of simple foams could not express the structure of real foams. Hooman et al.[14] investigated the effects of thermal scattering on the convection in a tube with a saturated porous medium. They showed that using reverse flow and obtaining a closed shape to temperature distribution could have accuracy and error of up to 5%. Shafii and Keshavarz[15] experimentally investigated the forced convection of a ferromagnetic fluid in a channel with a magnetic and non-magnetic porous medium. Their results showed that the percentage of increase in convective heat transfer coefficient in a magnetic porous medium is 38.66%, while for a non-magnetic porous medium it is 36.13%. Dehghan et al.[16] analytically investigated the developing flow in a channel filled with a porous medium. For the first time, they provided a relationship for the entrance length in a channel filled with a porous medium. Chen et al.[17] simulated the convection of nanofluids in the space between two concentric cylinders. Their results showed that at $\phi = 10\%$, heat transfer increased by 23%. Barnoon and Toghraie[18] investigated the forced convection in space between concentric cylinders, part of which was the porous medium. They found that the porous medium significantly increased heat transfer. Shen et al.[19] investigated forced convection in a micro heat sink with different porous foams. They found that the effect of the arrangement and location of the porous foam had a significant effect on the temperature and heat transfer properties. Lu et al.[20] proposed an analytical solution for forced convection in the space between two parallel plates, part of which was a porous medium. They found that the effect of porosity on heat transfer was directly related to the increase in foam thickness from the channel floor. Also, several studies focusing on fluid flow and heat transfer and the types of microtubes, microchannels, and nanofluids, including properties, behavior, and other parameters were reviewed by many researchers[21–39].

In many of these references, the authors have tried to increase the heat transfer rate with one of several factors mentioned above. Although much attention has been paid to the use of different nanofluids and their effects on heat transfer and the filling of microchannels from the porous medium, unfortunately very little attention has been paid to the placement of the rotating cylinder. The rotation of the cylinders and increasing their number is an innovation of this article.

Governing equations and solution method

Problem statement.   In this study, the effect of ϕ, Reynolds number, and porosity of porous medium in a microchannel filled with porous medium containing rotating cylinders on the flow field, heat transfer, and entropy generation are investigated. To solve the problem numerically, the CFD method and the finite volume model are used. For higher solution accuracy, the second-order UPWIND method is used and the SIMPLE algorithm is used to couple the pressure and velocity. Also, two-phase mixture model is used. The geometry studied in this research is a two-dimensional microchannel with a diameter of D = 200 μm and a length of L = 400 mm, which is filled with a porous medium (see Table 1). The effect of the porous medium placed in the microchannel is analyzed using the Brinkman model at different porosity percentages. In this research, different geometries have been named as a simple microchannel, geometric case A, microchannel with step, geometric case B, and microchannel containing rotating cylinders, geometric case C. The schematic of the problem is shown in Figs. 1,

Geometric case	L (mm)	D (μm)	S (mm)	E (mm)	H (μm)	d (μm)	f (mm)
A	400	200	–	–	–	–	–
B	400	200	320	80	20	–	–
C	400	200	320	80	20	150	63.88

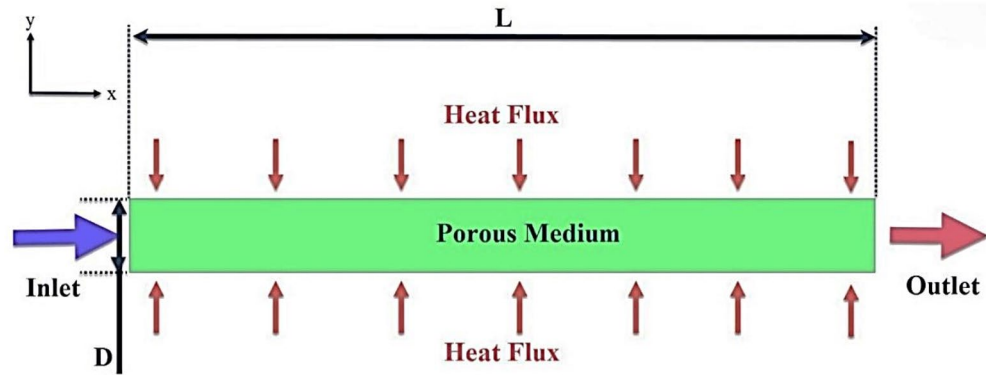**Table 1.** Dimensions of geometric cases.
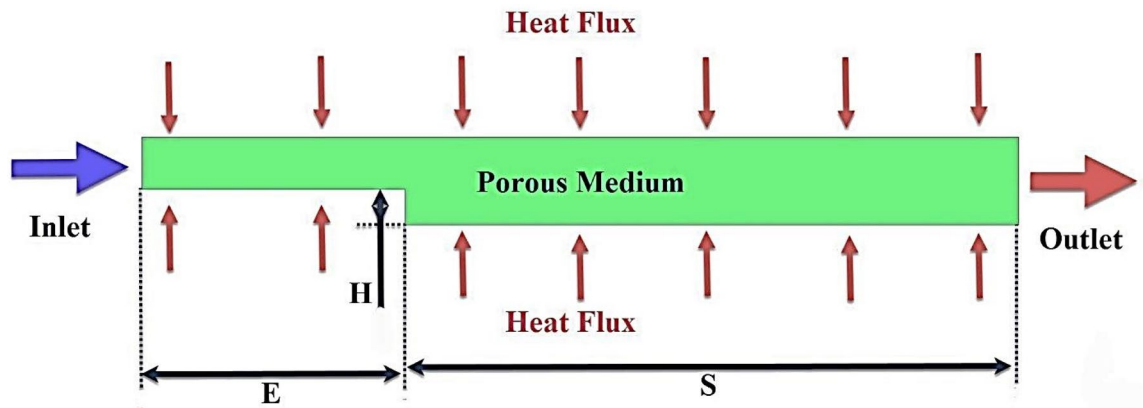

Figure 1. Schematic case A.

Figure 2. Schematic of case B.

2 and 3. Figure 2 shows the microchannels with step and Fig. 3 shows the microchannels with step and rotating cylinders. The working fluid at 300 K, Re = 250, 500, 750, and 1000 and $\phi = 0$, 1, and 2% enters the microchannel filled with a porous medium with $\varepsilon = 45$ and 90%. The nanoparticles used in this research are iron oxide and the base fluid is also water. The thermophysical properties of which are given in Table 2. A constant heat flux of 10,000 Wm^{-2} is applied to the lower wall of the microchannel.

Governing equations. In this research, the Eulerian two-phase mixture model is used to model the water-iron oxide nanofluids. To analyze the porous parts, the Brinkman model, which, unlike the Darcy model, is directly dependent on porosity and viscosity, uses the Local Thermal Equilibrium (LTE) method, in which the temperature of the fluid is equal to the solid surface.

– *Continuity equation* [41]

$$\overrightarrow{\nabla} \cdot \left(\rho_m \overrightarrow{V}_m \right) = 0,$$ (1)

– *Momentum equation* [41]
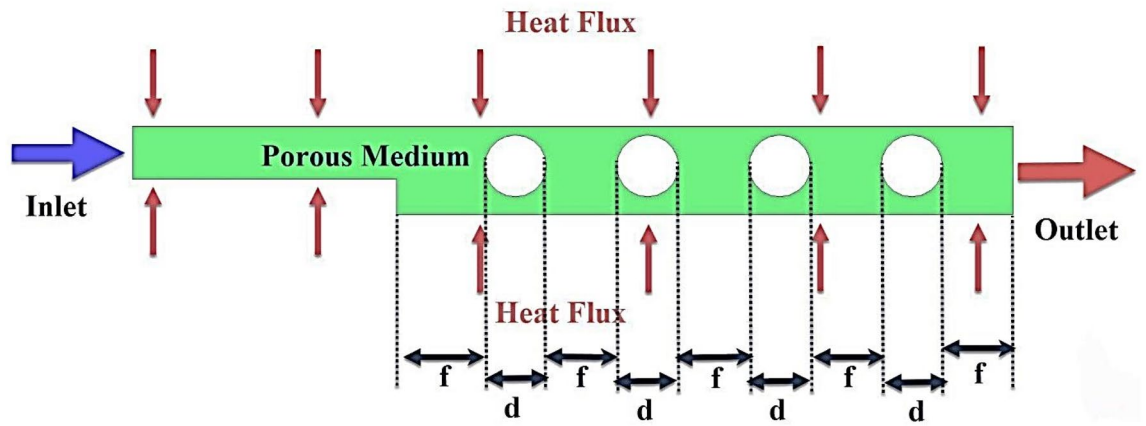
Figure 3. Schematic of case C.

$\mu\ [kg\ m^{-1}\ s^{-1}]$	$k\ [W\ m^{-1}\ K^{-1}]$	$C_p\ [J\ kg^{-1}\ K^{-1}]$	$\rho\ [kg\ m^{-3}]$	
0.001003	0.6	4182	998.2	Water
–	6	670	5200	Iron oxide

Table 2. Thermophysical properties of nanoparticles and base fluid[40].

$$\vec{\nabla}.\left(\rho_m \vec{V}_m \vec{V}_m\right) = -\vec{\nabla}P + \vec{\nabla}.\left(\mu_m\left(\vec{\nabla}\vec{V}_m + \vec{\nabla}\vec{V}_m^T\right) + \vec{\nabla}.\left[\sum_{k=1}^{n}\phi_k\rho_k\vec{V}_{dr,k}\vec{V}_{dr,k}\right]\right) \\ + \left(\frac{\varepsilon\mu_m}{K} + \frac{\rho_m\varepsilon^2 C_f}{\sqrt{K}}\left|\vec{V}_m\right|\right)\vec{V}_m, \tag{2}$$

where ρ_m is the density of the mixture, μ_m is the effective viscosity of the mixture, $\vec{V}_m$ is the velocity vector of the mixture, $\vec{V}_{dr,k}$ is the velocity vector of the secondary phase, and C_f is the shape function. Also,

$$\vec{V}_{dr,k} = \vec{V}_k - \vec{V}_m, \tag{3}$$

$$C_F = 0.55\left(1 - 5.5\frac{L}{D_h}\right). \tag{4}$$

– *Energy equation* [40]

$$\vec{\nabla}\left(\sum_{k=1}^{n}\left(\rho_k C_{p,k}\right)\phi_k\varepsilon\vec{V}^k T\right) = \vec{\nabla}.k_m\vec{\nabla}T, \tag{5}$$

Drift velocity:

$$\vec{V}_{dr,k} = \vec{V}_{pf} - \sum_{k=1}^{n}\frac{\phi_k\rho_k}{\rho_m}\vec{V}_{f,k}, \tag{6}$$

The mixture velocity[40]:

$$\vec{V}_m = \frac{\sum_{k=1}^{n}\phi_k\mu_k\vec{V}_k}{\rho_m}, \tag{7}$$

The density of the mixture[40]:

$$\rho_m = \sum_{k=1}^{n}\phi_k\rho_k, \tag{8}$$

The viscosity of the mixture[40]:

$$\mu_m = \sum_{k=1}^{n} \phi_k \mu_k, \tag{9}$$

and

$$\overrightarrow{V}_{pf} = \frac{\rho_p d_p^2 (\rho_p - \rho_m)}{18 \mu_f f_{drag} \rho_p} \left(\overrightarrow{g} - \left(\overrightarrow{V}_m . \overrightarrow{\nabla} \right) \overrightarrow{V}_m \right), \tag{10}$$

$$f_{drag} = \begin{cases} 1 + 0.15 \mathrm{Re}^{0.687} & [\mathrm{Re} \leq 1000] \\ 0.0183 \mathrm{Re} & [\mathrm{Re} > 1000] \end{cases} \tag{11}$$

Therefore, the drift velocity is obtained as a function of relative velocity as follows[40],

$$\overrightarrow{V}_{dr,k} = \overrightarrow{V}_{pf} - \sum_{k=1}^{n} \left[\frac{\phi_k \rho_k}{\rho_m} \overrightarrow{V}_{f,k} \right]. \tag{12}$$

Thermophysical properties of nanofluid[40].

$$\rho_m = (1 - \phi)\rho_f + \phi \rho_{np}, \tag{13}$$

$$(\rho C_p)_m = (1 - \phi)(\rho C_p)_f + \phi (\rho C_p)_{np}, \tag{14}$$

$$\mu_m = \frac{\mu_f}{(1 - \phi)^{2.5}}, \tag{15}$$

$$k_m = k_f \left[1 + 2.72\phi + 4.97\phi^2 \right]. \tag{16}$$

Entropy generation. *Entropy generation due to heat transfer per unit volume[40],*

$$S_{gen,HT}''' = \frac{k_m}{T^2} \left[\left(\frac{\partial T}{\partial x} \right)^2 + \left(\frac{\partial T}{\partial y} \right)^2 \right], \tag{17}$$

Entropy generation due to friction per unit volume [40],

$$S_{gen,f}''' = \frac{\mu_m}{T} \left[2 \left(\left(\frac{\partial u}{\partial x} \right)^2 + \left(\frac{\partial v}{\partial y} \right)^2 \right) + \left(\frac{\partial u}{\partial y} + \frac{\partial v}{\partial x} \right)^2 \right], \tag{18}$$

Total entropy generation:

$$S_{gen,HT} = \int S_{gen,HT}''' dV, \tag{19}$$

$$S_{gen,f} = \int S_{gen,f}''' dV, \tag{20}$$

$$S_{gen,Tot} = \int S_{gen,T}''' dV + \int S_{gen,F}''' dV. \tag{21}$$

Measurement parameters.

– *Dimensionless parameters*

$$X = \frac{x}{L}, Y = \frac{y}{h}, U = \frac{u}{u_{in}}, \Omega = \frac{\omega H}{2\nu}, \tag{22}$$

where x represents the direction of flow and L represents the length of the microchannel.

– *Reynolds number:*

$$\mathrm{Re} = \frac{\rho_m V_{in} L}{\mu_m}, \tag{23}$$

– *Pressure drop:*

$$\Delta P = \frac{fL\rho_m V_{in}^2}{2L}, \tag{24}$$

– *Friction factor:*

$$C_f = \frac{\tau_w}{\frac{1}{2}\rho_m V_{in}^2}, \tag{25}$$

– *Wall temperature and bulk temperature of nanofluid:*

$$T_w(x) = \frac{1}{A}\int T dA, \tag{26}$$

$$T_b(x) = \frac{\int T\rho_m |Vd\vec{A}|}{\int \rho_m |Vd\vec{A}|}, \tag{27}$$

$$h(x) = \frac{q''(x)}{T_w(x) - T_b}, \tag{28}$$

$$h = \frac{1}{L}\int_0^L h(x)dx, \tag{29}$$

$$Nu(x) = \frac{h(x)L}{k_m}, \tag{30}$$

$$Nu_{ave} = \frac{hL}{k_m}, \tag{31}$$

– *Performance Evaluation Criterion (PEC)* [42]

$$PEC = \frac{Nu/Nu_s}{\left(f/f_s\right)^{\frac{1}{3}}}. \tag{31}$$

Boundary conditions.

(A) Inlet conditions:

The inlet velocity is calculated based on the Reynolds number and the properties of the nanofluid, and the inlet temperature is also constant.

(B) Outlet conditions:

We do not have temperature conditions and the outlet pressure is equal to the atmospheric pressure.

(C) Conditions of the walls:

A constant heat flux of 10,000 Wm^{-2} is applied to the upper wall.

Assumptions.

- The flow is steady.
- Viscous dissipation is ignored.
- The base fluid flow is incompressible.
- The base fluid is Newtonian.
- The no-slip condition and no temperature jump are applied in the solid walls.

Grid independency and validation.   In Fig. 4, a structured grid is used by increasing the number of elements perpendicular to the wall. The independency of the obtained solution from the grid is evaluated at constant heat flux, Re = 200, ϕ = 0% and ε = 45% with Nu_{ave} and continues when the error of each stage falls below 3% compared to the previous stage. Figure 5 shows the Nu_{ave} versus the number of the grids. In the mentioned figures, the difference of Nu_{ave} in points 3 and 4 has reached below 3%; so, point 3 is selected as the desired computational mesh. To ensure the accuracy of the obtained numerical results, it is necessary to compare the obtained numerical results with the valid results of other researchers. For this purpose, Ref.[43] has been used as
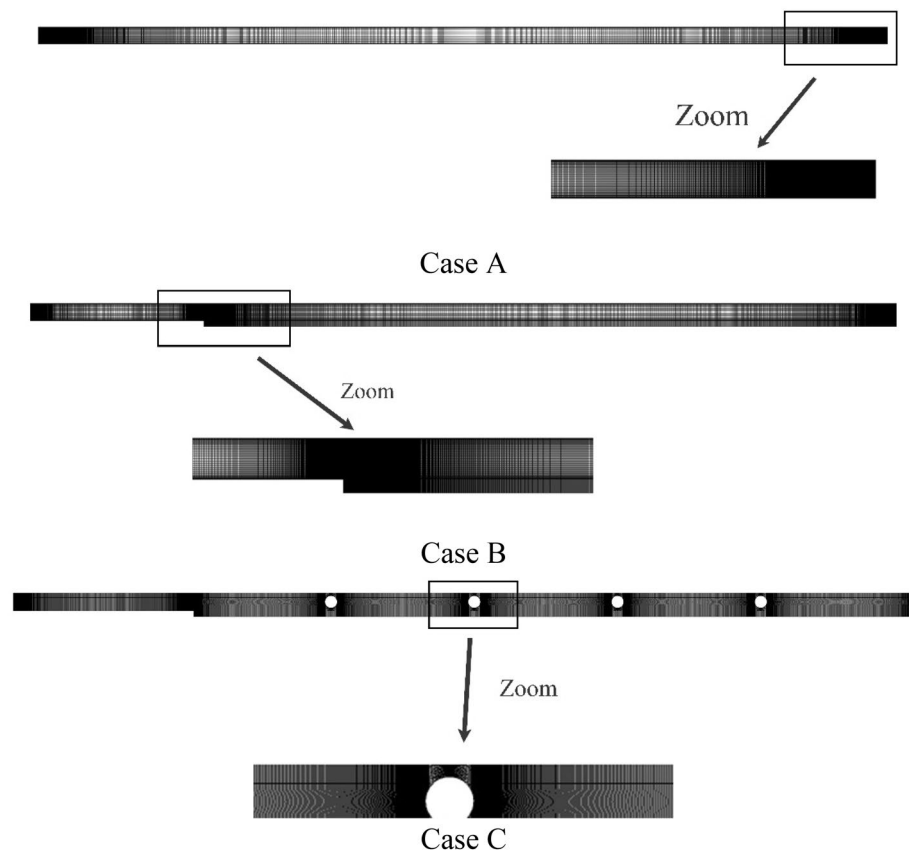
Figure 4. Computational grid.

the validation reference in Fig. 6. In this reference, half of the velocity profiles at the output are compared with a Re = 200, a porosity of 45%, and ϕ = 1%. Because the obtained numerical results are consistent with the experimental results and the error is less than 2%, so the process of numerical problem solving has good accuracy.

Results and discussion

Effect the ϕ on ΔP. Figure 7 shows the ΔP versus the ϕ. Increasing the ϕ increases the density of the working fluid and due to the direct relationship between the Reynolds number and the density of the working fluid, with increasing the Reynolds number, the ΔP also increases. Comparing different geometric cases, it can be said that case C, which increases the Reynolds number locally by rotating the cylinders, ultimately increases the ΔP compared to case B. On the other hand, in case B, the presence of a step inside the two-dimensional microchannel increases the cross-sectional area and decreases the Reynolds number, which is a significant decrease, and in general, in case B, we see less ΔP than case A. By comparing the ΔP in different Reynolds numbers, we can say that due to the increase in the number of input Reynolds and consequently the inlet speed, we see more ΔP in all geometric cases. Comparing porosity percentages with each other, the ΔP at $\varepsilon = 90\%$ is greater than the ΔP at $\varepsilon = 45\%$. The reason for this phenomenon is that there is more free space at $\varepsilon = 90\%$ for the passage of nanofluids and the movement of nanofluids is less with obstacles and the velocity is higher and as a result, the ΔP in $\varepsilon = 90\%$ is higher than $\varepsilon = 45\%$.

Effect of ϕ on $C_{f,ave}$. Figure 8 shows the $C_{f,ave}$ versus ϕ, at different Reynolds numbers, porosity percentages, and geometric cases. As can be seen, with increasing the ϕ, the $C_{f,ave}$ increases. This is due to the increase in the density and viscosity of the nanofluid, which increases the $C_{f,ave}$. Comparing different geometric cases, it becomes clear that the highest values of the $C_{f,ave}$ have the geometric case C. The reason for this phenomenon is the creation of velocity gradients near the wall due to the rotational motion of the cylinders. On the other hand, geometric case B shows a higher $C_{f,ave}$ than geometric case A due to the presence of steps and increase in velocity gradients. By comparing the porosity percentages with each other, it is concluded that due to the greater contact of the nanofluid with the porous medium and the creation of higher velocity gradients, the porosity percentage is 45% and the values of $C_{f,ave}$ are 90% higher than the porosity percentage. In Fig. 8, with increasing the ϕ, the $C_{f,ave}$ in the geometric case C in Re = 200 increases by 5.221, 6.95, and 11.103%, respectively, in Re = 400 increases by 5.962, 6.949 and 11.453, in Re = 600 increases by 5.499, 6.408 and 11.116% respectively and in Re = 800 increases by 5.354, 6.196 and 11.813% respectively. By increasing the ϕ, the $C_{f,ave}$ in the geometric case B increases in Re = 200 by 5.193, 6.977 and 11.078%, respectively, in Re = 400 increases by 5.663, 6.892 and 11.157%, respectively, in Re = 600 increases by 531.5, 6.376 and 11.249% respectively and in Re = 800 increases

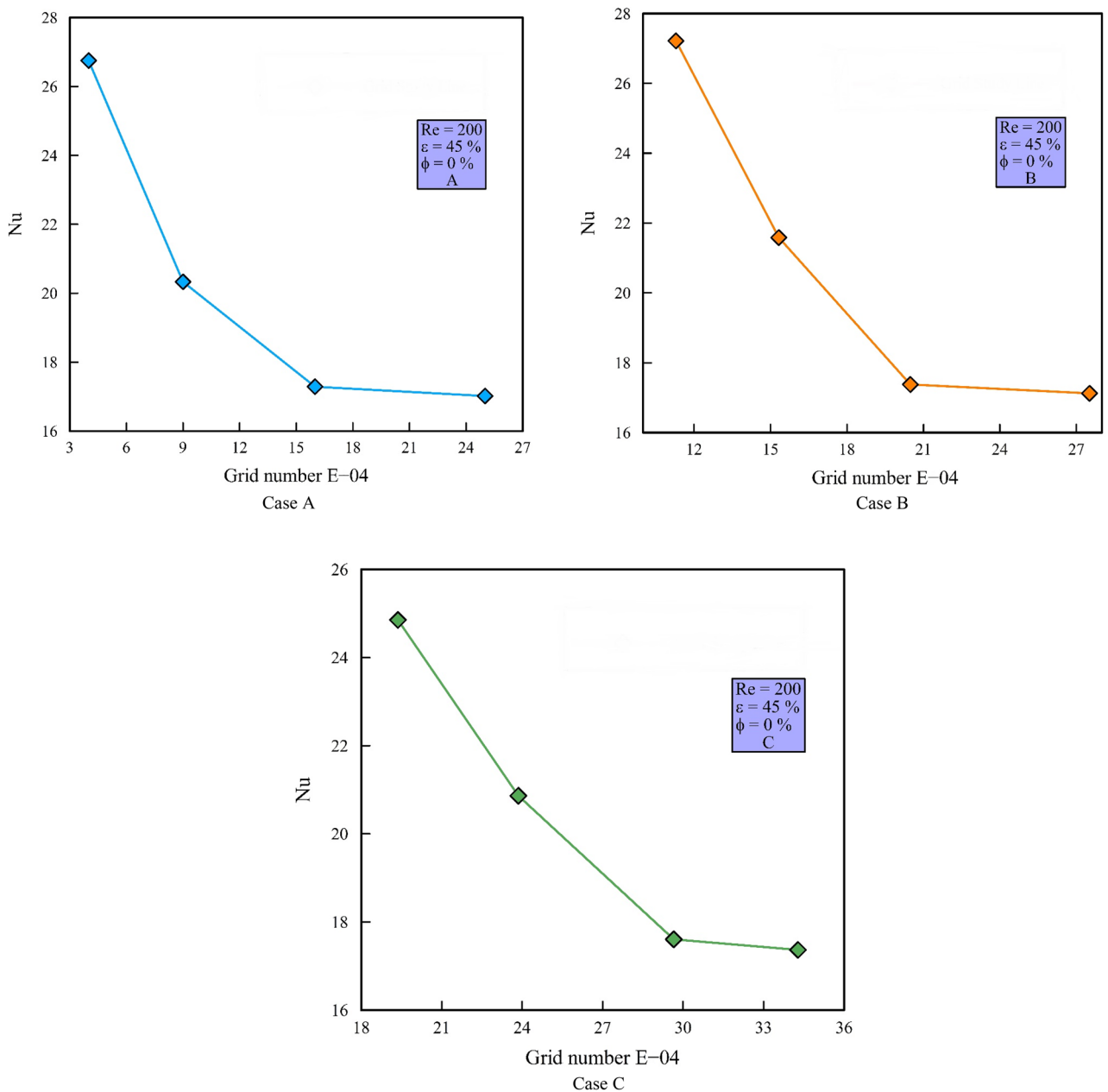**Figure 5.** Grid independency diagrams.

by 7.548, 6.436 and 11.984% respectively. The $C_{f,ave}$ in the geometric case A with increasing the ϕ in Re = 200 increases by 5.69, 7.313 and 16.311%, respectively, in Re = 400 increases by 5.892, 7.292 and 16.296%, respectively, in Re = 600 increases by 5.819, 7.115 and 16.283% respectively and in Re = 800 it increases by 3.11, 7.155 and 16.261%, respectively.

Effect of ϕ on Nu_{ave}.   Figure 9 shows the Nu_{ave} versus ϕ in different Reynolds numbers, porosity percentages, and geometric cases. As can be seen, with increasing ϕ and Reynolds number, the Nu_{ave} increases. This behavior can be examined from both mathematical and physical perspectives. As the Reynolds number increases, the velocity increases, and thus the thickness of the thermal boundary layer decrease. From a mathematical point of view, reducing the temperature difference, which is associated with decreasing the thickness of the thermal boundary layer, increases the Nu_{ave}. In general, the Nu_{ave} indicates the ratio of convection to conduction heat transfer. For this reason, in convection heat transfer, this ratio is always greater than one. Due to the increase in surface area, which itself increases the convective heat transfer coefficient, the Nu_{ave} in $\varepsilon = 45\%$ is higher than $\varepsilon = 90\%$. Comparing different geometries with each other, it can be seen that the geometric case B shows lower Nu_{ave} values than geometric case A due to the presence of steps and local decrease of Reynolds number. However, this is not the case for geometric case C with different non-dimensional rotational velocities because the rotational motion increases the Reynolds number locally and consequently the local velocity and
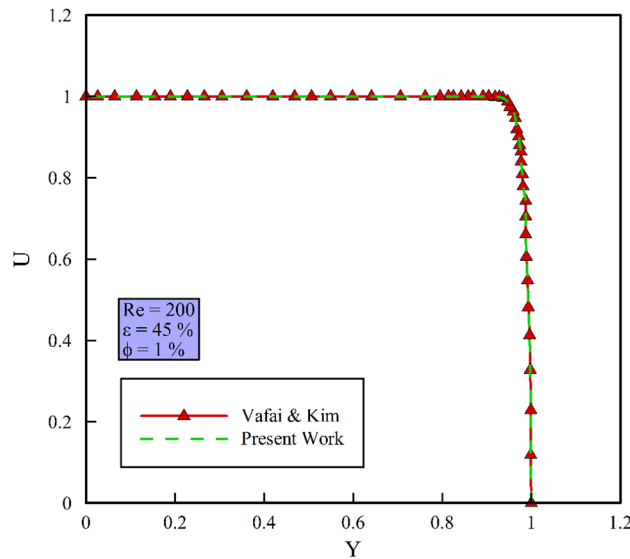
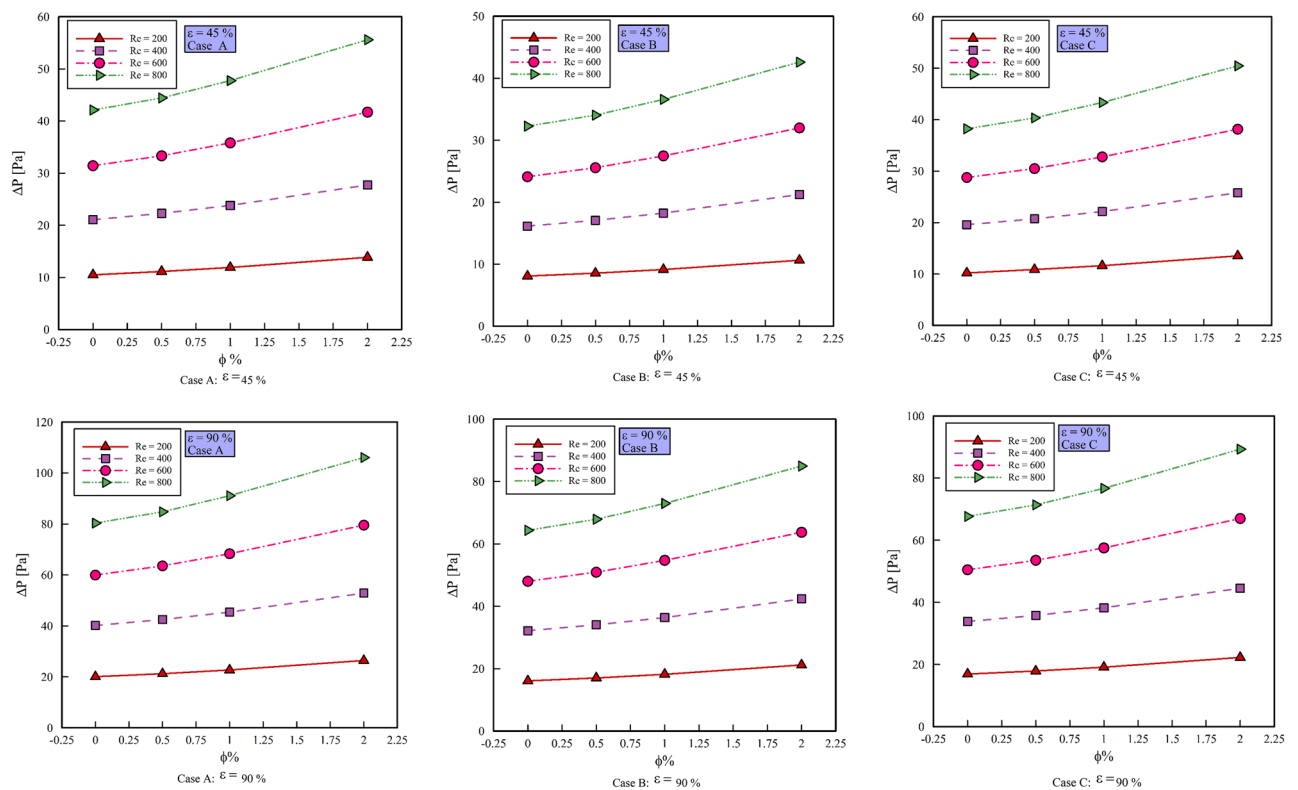**Figure 6.** Validation diagram and comparison of the present work with Ref.[43].

Figure 7. ΔP versus ϕ.

shows higher values of the Nu_{ave} than the geometric case A. Also, in geometric case C, with the increase of the non-dimensionless rotational velocity of the rotating cylinders, we see an increase of the local Reynolds number more than before, and this causes a further increase of the Nu_{ave}.

Performance Evaluation Criterion (PEC).   Figure 10 shows the PEC versus ϕ in different Reynolds numbers, porosity percentages and geometric cases. For the above reasons, increasing the porosity percentage reduces the heat transfer and consequently the PEC values. Placing the rotating cylinders in geometric case C causes the PEC to have an increasing trend compared to other geometric cases. In general, values of PEC above
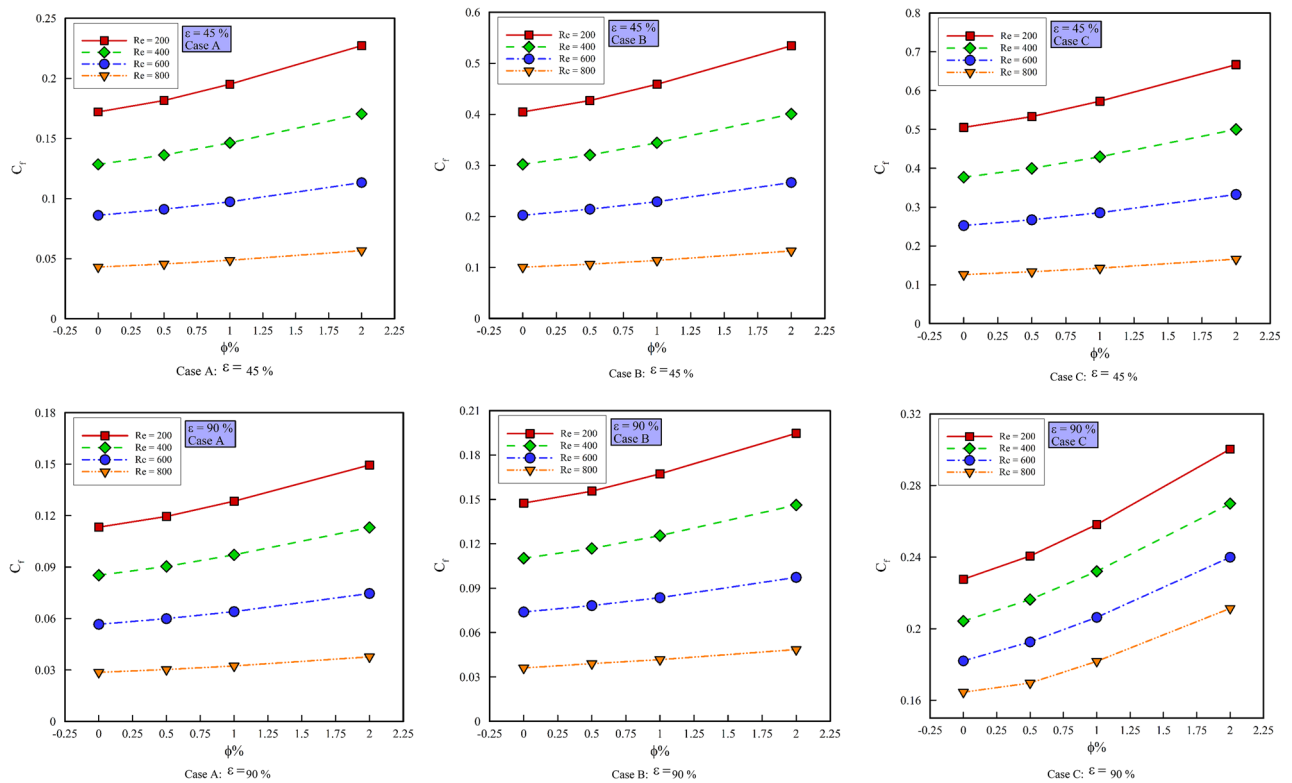
Figure 8. $C_{f,ave}$ versus ϕ.

1 are known as favorite PEC values. As can be seen, all the values in the mentioned figures have values higher than one, although the PEC changes with the ϕ are small. Increasing the ϕ in the geometric case A increases the PEC in Re = 200 by 20.12, 1.67 and 1.074%, respectively, in Re = 400 by 2.49, 1.518 and 1.563%, respectively, in Re = 600 is 2.758, 0.954 and 1.404%, respectively, and in Re = 800 is 2.982, 1.399 and 1.338%, respectively. Increasing the ϕ in geometric case B increases PEC in Re = 200 by 20.139, 1.657 and 1.065%, respectively, in Re = 400 by 2.83, 1.328 and 1.556%, respectively, in Re = 600 by 2.766, 1.054 and 1.397%, respectively, and in Re = 800 by 2.891, 1.072 and 1.867%, respectively.

Effect of ϕ on entropy generation.   Figure 11 shows the entropy generation due to heat transfer ($S'''_{gen,HT}$) versus ϕ and Fig. 12 shows the entropy generation due to friction ($S'''_{gen,f}$) versus ϕ. All the figures are presented at different Reynolds numbers, porosity percentages, and geometric cases. As can be seen, with increasing ϕ and Reynolds number, $S_{gen,HT}$ decreases. This is due to the reduction of the thermal boundary layer and the reduction of temperature gradients. As can be seen, increasing the Reynolds number and the ϕ increases the $S'''_{gen,f}$. In general, increasing the porosity percentage reduces $S'''_{gen,f}$ and $S_{gen,HT}$. Increasing the ϕ in case A reduces the $S_{gen,HT}$ in Re = 200 by 0.402, 0.906 and 0.741%, respectively, in Re = 400 by 0.945, 0.599 and 0.324%, respectively, in Re = 600 by 0.577, 0.121 and 0.116% respectively and in Re = 800 by 0.041, 0.244 and 1.169% respectively. Increasing the ϕ in geometric case B reduces the $S_{gen,HT}$ in Re = 200 by 0.391, 0.495 and 1.119%, respectively, in Re = by 095, 0.119 and o.272%, respectively, in Re = 600 by 0.064, 0.094 and 0.178%, respectively, and in Re = 800 by 0.05, 0.1 and 0.2%, respectively. Increasing the ϕ in the geometric case B increases the $S'''_{gen,f}$ in Re = 200 by 7.231, 9.461 and 23.39%, respectively, in Re = 400 by 7.19, 9.41 and 23.33%, respectively, in Re = 600 by 7.57, 10.678 and 23.171%, respectively, and in Re = 800 by 6.631, 10.667 and 23.147%, respectively. Increasing the ϕ in the geometric case C increases the $S'''_{gen,f}$ in Re = 200 by 8.654, 9.235 and 18.847%, respectively, in Re = 400 by 7.227, 9.162 and 18.696%, respectively, in Re = 600 by 7.215, 9.156 and 18.649% respectively and in Re = 800 by 7.185, 9.143 and 18.621%, respectively.

Study of flow physics.   Figure 13 shows the streamlines at Re = 800, ϕ = 2%, and various geometric cases. As can be seen, the streamlines in the middle of the microchannel have a different color from the streamlines adjacent to the microchannel wall. By adding steps and placing rotating cylinders, the shape of the streamlines changes. Figure 14 shows the temperature contour at Re = 800, ϕ = 2%, and various geometric cases. As can be seen, placing the rotating cylinders inside the microchannel disturbs the thermal dissipation pattern relative to the geometric case A. Figure 15 shows the velocity contour at Re = 800, ϕ = 2%, and various geometric cases. By placing the step in the microchannel, the flow pattern changes, and the local velocity decreases. Also, placing the rotating cylinders in the microchannel causes the amount of velocity around the cylinders to change.
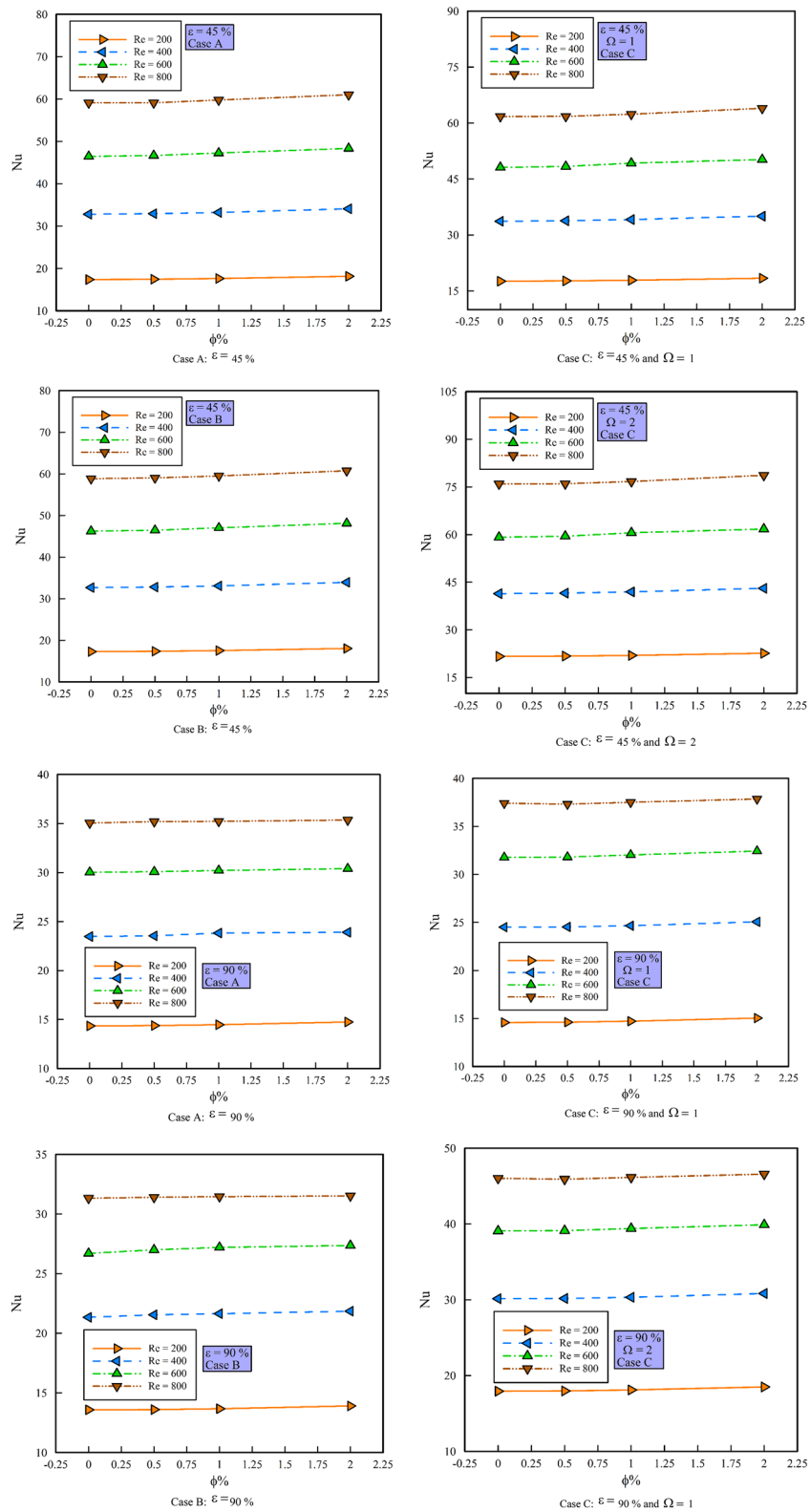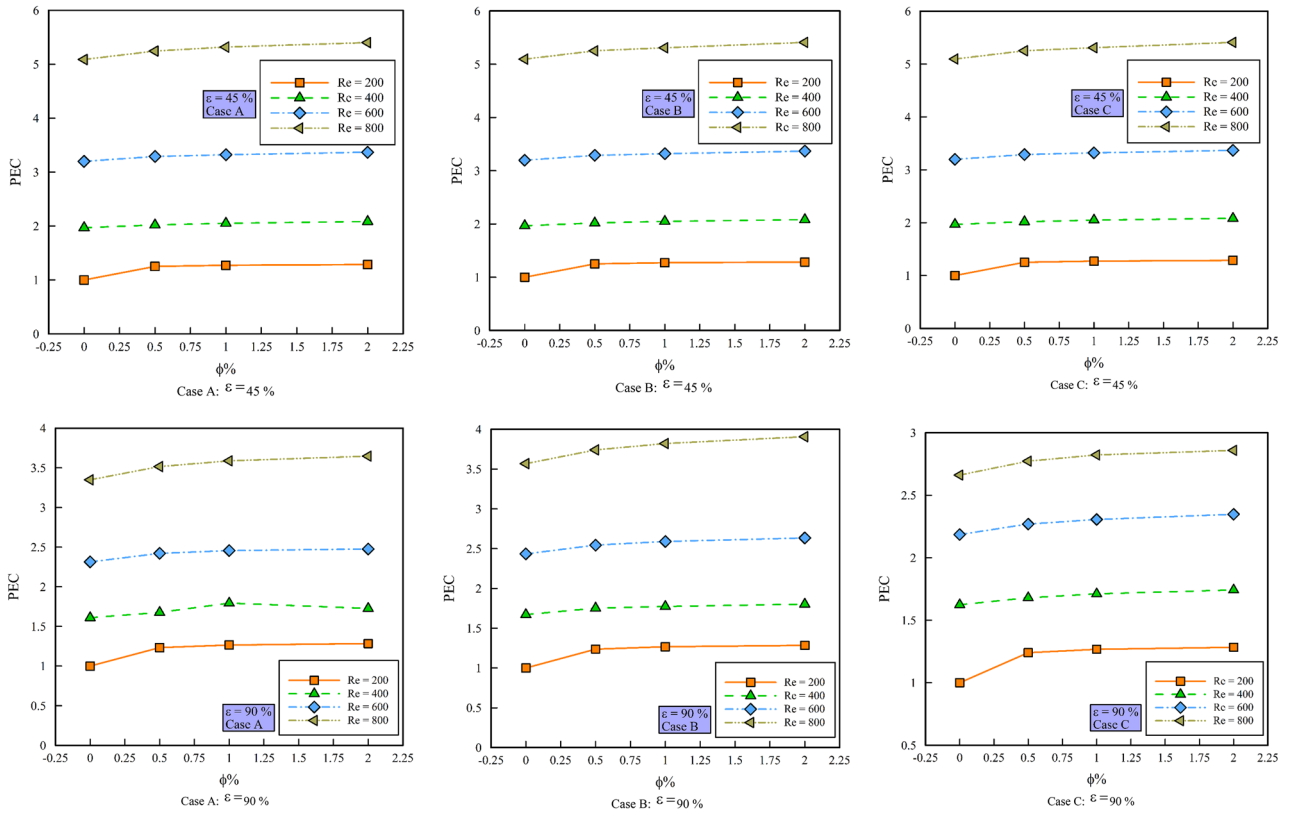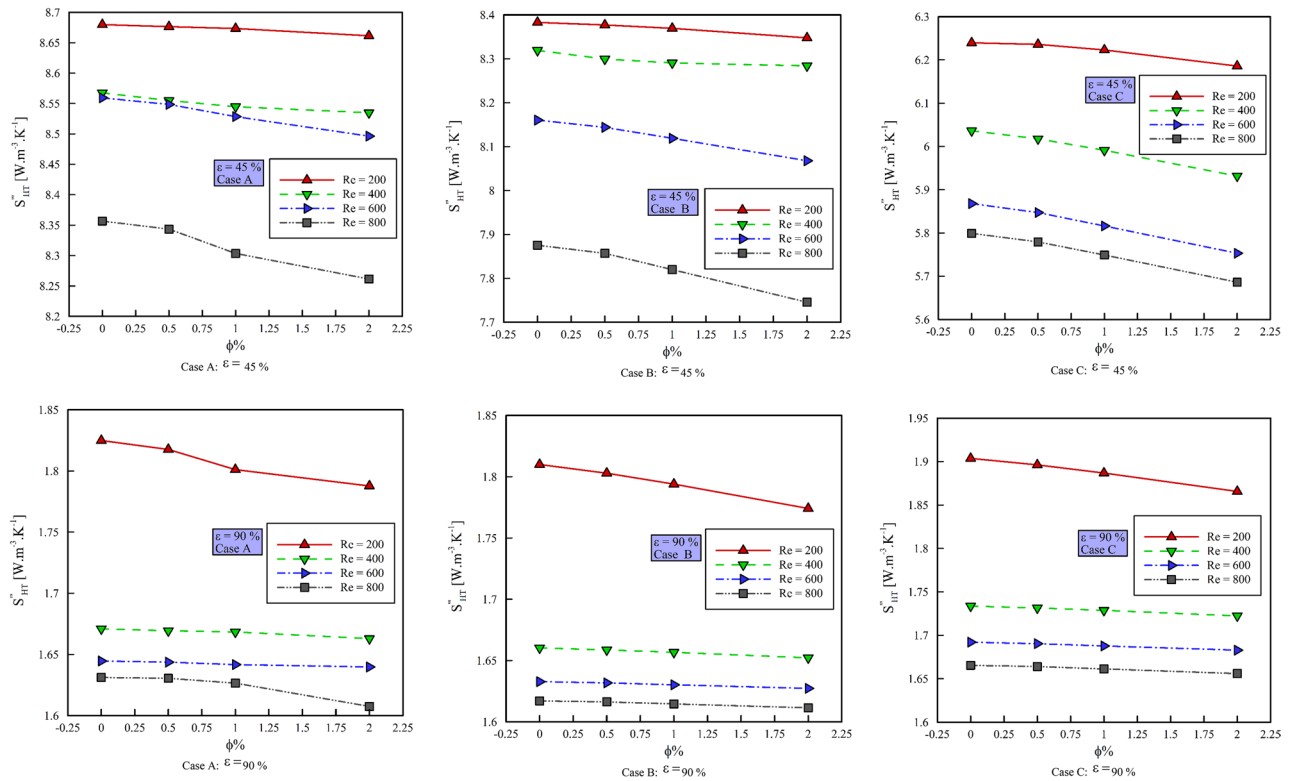
Figure 9. Nu_{ave} versus ϕ.

Figure 10. PEC versus ϕ.

Figure 11. $S_{gen,HT}$ versus ϕ in different Reynolds numbers and porosity percentages.
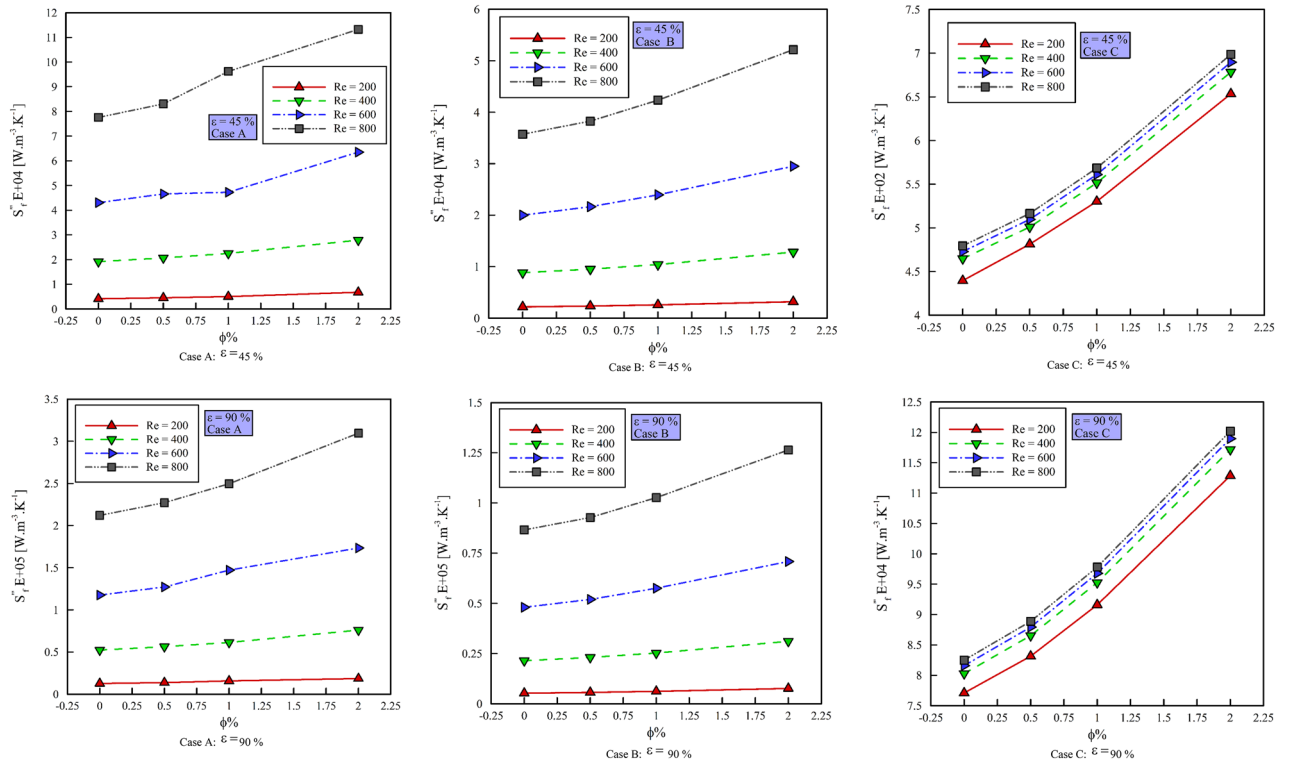
Figure 12. $S'''_{gen,f}$ versus ϕ in different Reynolds numbers and porosity percentages.

Conclusion

The results extracted from the numerical simulation include the following:

- Increasing the Reynolds number increases the heat transfer.
- The use of nanoparticles improves the thermophysical properties of the base fluid.
- Reducing the porosity percentage reduces the heat transfer because the contact surface decreases.
- Increasing the Reynolds number leads to a decrease in the $C_{f,ave}$.
- Increasing the ϕ increases the $C_{f,ave}$ due to the increase in viscous forces.
- Increasing the ϕ has little effect on $S'''_{gen,HT}$.
- Increasing the dimensionless rotational velocity of rotating cylinders increases the Nu_{ave}.
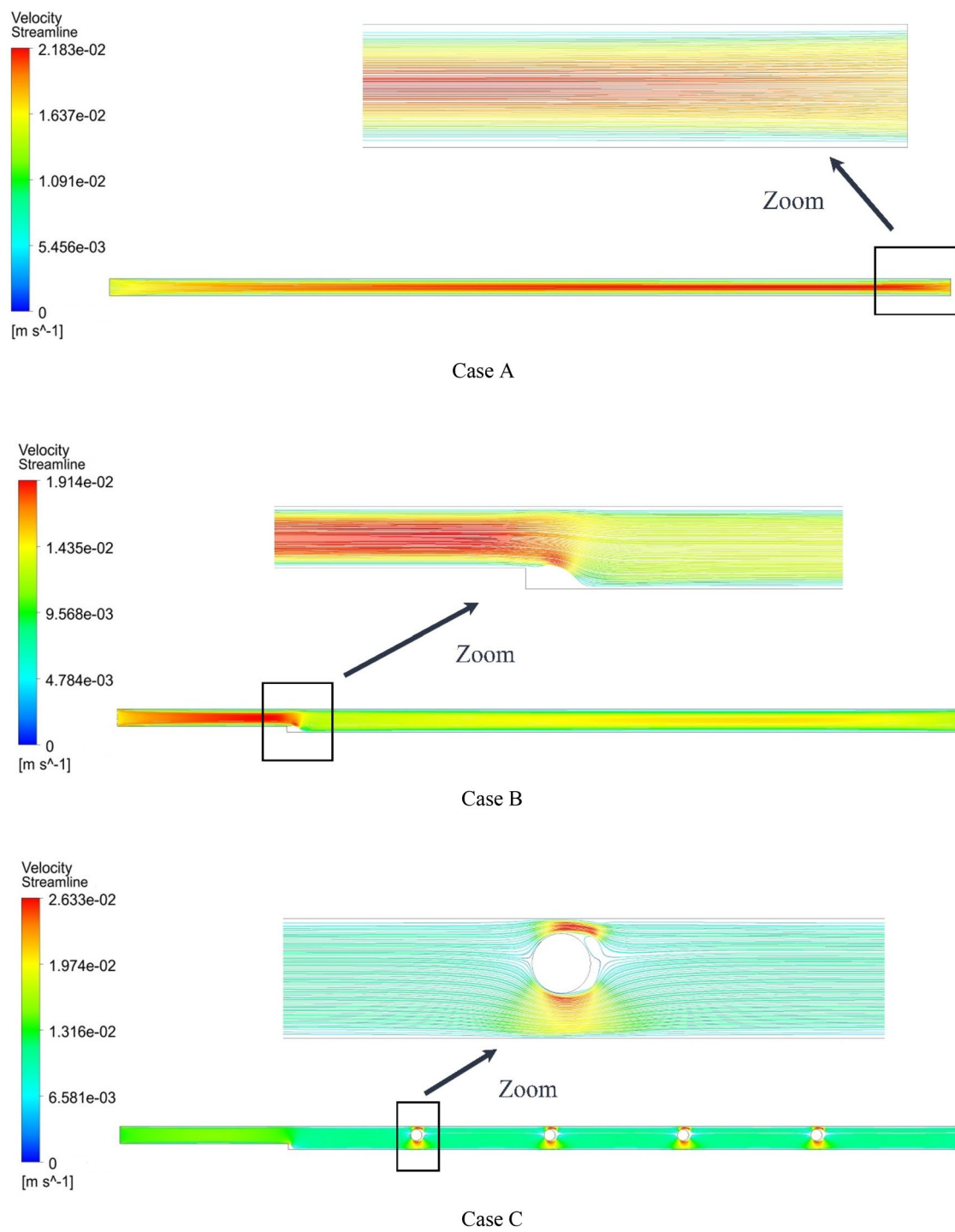- Increasing the ϕ does not have much effect on Nu_{ave}.

Case A

Case B

Case C

Figure 13. Streamlines in $Re = 800, \phi = 2$.
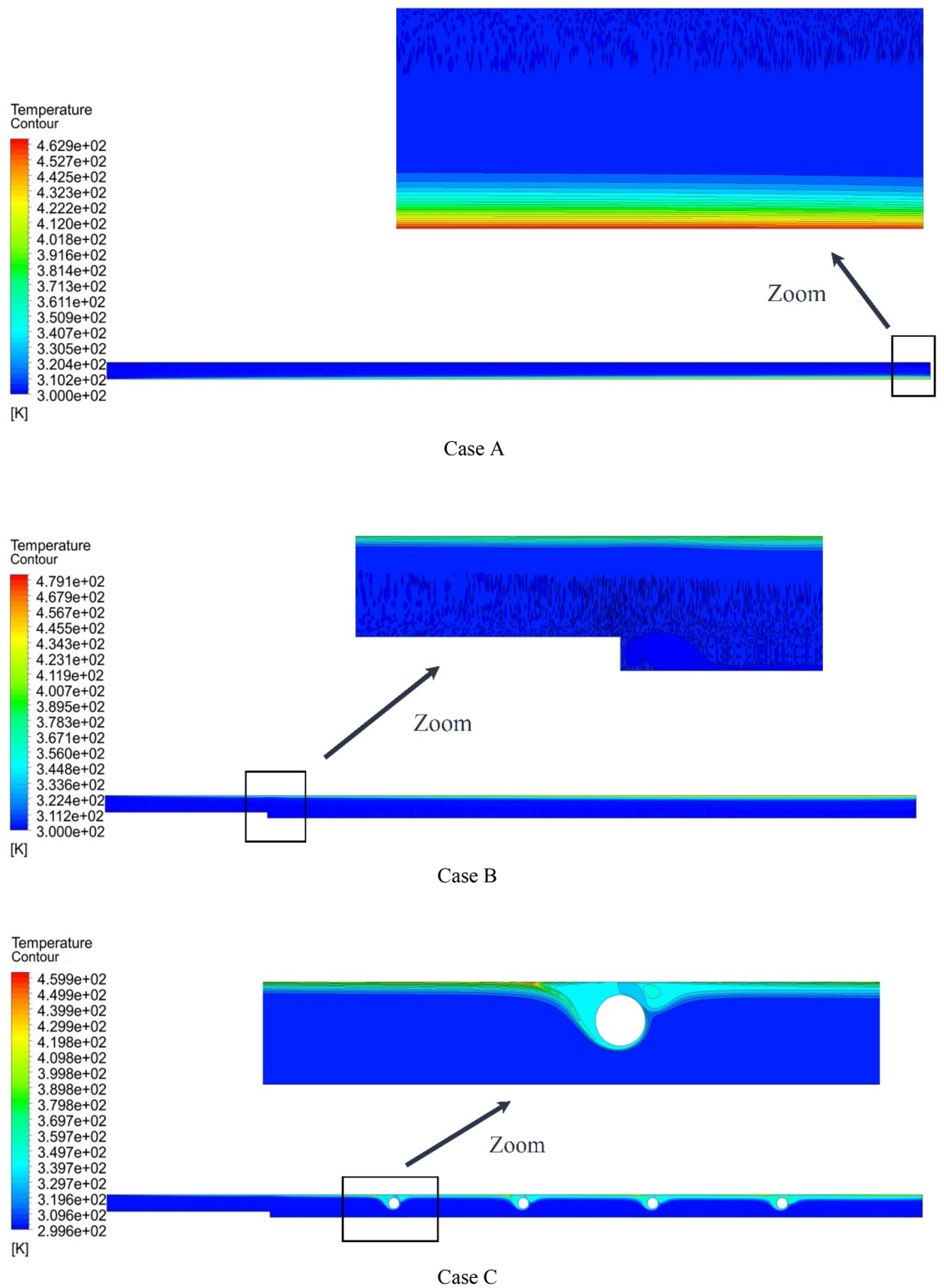
Figure 14. Temperature contours in Re = 800, $\phi = 2\%$.

Case A

Case B

Case C
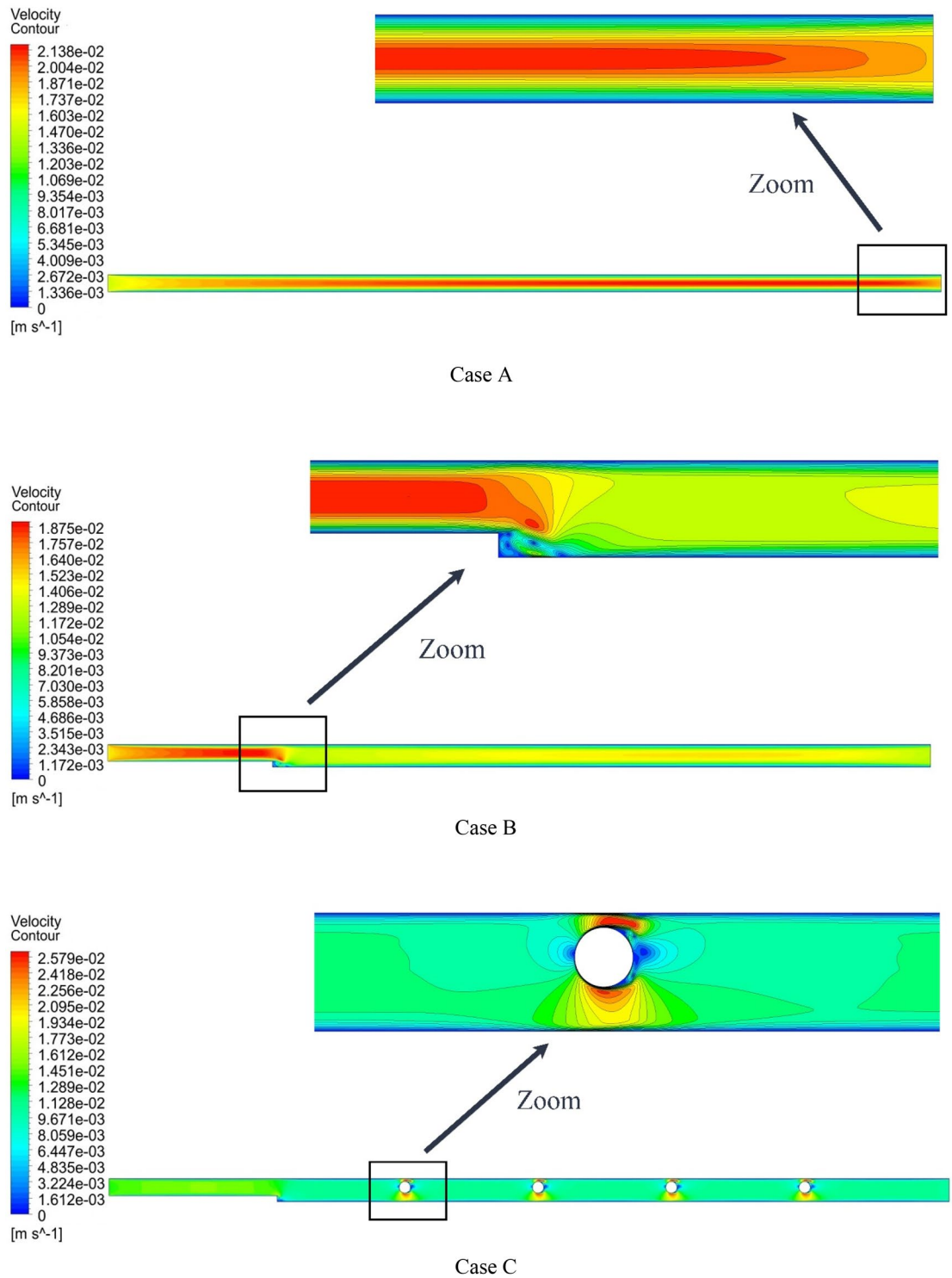
Figure 15. Velocity contours at Re = 800, $\phi = 2\%$.

References

1. Tuckerman, D. B. & Pease, R. F. W. High-performance heat sinking for VLSI. *IEEE Electron Device Lett.* **2**(5), 126–129 (1981).
2. D. a Nield and A. Bejan, *Convection in Porous Media Third Edition*, vol. 24. 2006.
3. Fadaei, F., Shahrokhi, M., Dehkordi, A. M. & Abbasi, Z. Forced-convection heat transfer of ferrofluids in a circular duct partially filled with porous medium in the presence of magnetic field. *J. Magn. Magn. Mater.* **475**, 304–315 (2019).

4. Wang, K. & Li, P. Forced convection in bidisperse porous media incorporating viscous dissipation. *Appl. Therm. Eng.* **140**, 86–94 (2018).

5. Li, P., Zhang, J., Wang, K. & Xu, Z. Heat transfer characteristics of thermally developing forced convection in a porous circular tube with asymmetric entrance temperature under LTNE condition. *Appl. Therm. Eng.* **154**, 326–331 (2019).

6. Xu, Z. G. & Gong, Q. Numerical investigation on forced convection of tubes partially filled with composite metal foams under local thermal non-equilibrium condition. *Int. J. Therm. Sci.* **133**, 1–12 (2018).

7. Baragh, S., Shokouhmand, H., Ajarostaghi, S. S. M. & Nikian, M. An experimental investigation on forced convection heat transfer of single-phase flow in a channel with different arrangements of porous media. *Int. J. Therm. Sci.* **134**, 370–379 (2018).

8. Li, P., Zhong, J., Wang, K. & Zhao, C. Analysis of thermally developing forced convection heat transfer in a porous medium under local thermal non-equilibrium condition: a circular tube with asymmetric entrance temperature. *Int. J. Heat Mass Transf.* **127**, 880–889 (2018).

9. Jamal-Abad, M. T., Saedodin, S. & Aminy, M. Variable conductivity in forced convection for a tube filled with porous media: A perturbation solution. *Ain Shams Eng. J.* **9**(4), 689–696 (2018).

10. Akyildiz, F. T. & Siginer, D. A. Exact solution for forced convection gaseous slip flow in corrugated microtubes. *Int. J. Heat Mass Transf.* **112**, 553–558 (2017).

11. Zeng, S., Kanargi, B. & Lee, P. S. Experimental and numerical investigation of a mini channel forced air heat sink designed by topology optimization. *Int. J. Heat Mass Transf.* **121**, 663–679 (2018).

12. Xu, Z. G., Qin, J., Zhou, X. & Xu, H. J. Forced convective heat transfer of tubes sintered with partially-filled gradient metal foams (GMFs) considering local thermal non-equilibrium effect. *Appl. Therm. Eng.* **137**, 101–111 (2018).

13. Vijay, D., Goetze, P., Wulf, R. & Gross, U. Homogenized and pore-scale analyses of forced convection through open cell foams. *Int. J. Heat Mass Transf.* **123**, 787–804 (2018).

14. Hooman, K., Li, J. & Dahari, M. Thermal dispersion effects on forced convection in a porous-saturated pipe. *Therm. Sci. Eng. Prog.* **2**, 64–70 (2017).

15. Shafii, M. B. & Keshavarz, M. Experimental study of internal forced convection of ferrofluid flow in non-magnetizable/magnetizable porous media. *Exp. Therm. Fluid Sci.* **96**, 441–450 (2018).

16. Dehghan, M., Valipour, M. S., Keshmiri, A., Saedodin, S. & Shokri, N. On the thermally developing forced convection through a porous material under the local thermal non-equilibrium condition: an analytical study. *Int. J. Heat Mass Transf.* **92**, 815–823 (2016).

17. Chen, W. C., Chen, Y. F. & Cheng, W. T. Numerical simulation on forced thermal flow of nanofluid in the gap between co-axial cylinders with rotational inner spindle. *Int. J. Heat Mass Transf.* **102**, 971–979 (2016).

18. Barnoon, P. & Toghraie, D. Numerical investigation of laminar flow and heat transfer of non-Newtonian nanofluid within a porous medium. *Powder Technol.* **325**, 78–91 (2018).

19. Shen, B., Yan, H., Sunden, B., Xue, H. & Xie, G. Forced convection and heat transfer of water-cooled microchannel heat sinks with various structured metal foams. *Int. J. Heat Mass Transf.* **113**, 1043–1053 (2017).

20. Lu, W., Zhang, T. & Yang, M. Analytical solution of forced convective heat transfer in parallel-plate channel partially filled with metallic foams. *Int. J. Heat Mass Transf.* **100**, 718–727 (2016).

21. Salman, B. H., Mohammed, H. A., Munisamy, K. M. & Kherbeet, A. S. Characteristics of heat transfer and fluid flow in microtube and microchannel using conventional fluids and nanofluids: a review. *Renew. Sustain. Energy Rev.* **28**, 848–880 (2013).

22. Chen, S.-B. *et al.* Combined effect of using porous media and nano-particle on melting performance of PCM filled enclosure with triangular double fins. *Case Stud. Therm. Eng.* **25**, 100939 (2021).

23. Bakhshy, H., Rohani, S. M. A., Heydari, P. & Asadi, R. Heat transfer and fluid flow analysis of a novel micro-miniature cryocooler model. *Adv. J. Chem. A* **1**(1), 32–38 (2018).

24. Sheikholeslami, M., Jafaryar, M. & Saleem, S. Zhixiong Li, Ahmad Shafee, Yu Jiangg, Nanofluid heat transfer augmentation and exergy loss inside a pipe equipped with innovative turbulators. *Int. J. Heat Mass Transf.* **126**(B), 156–163 (2018).

25. Li, Z., Sheikholeslami, M., Chamkha, A. J., Raizah, Z. A. & Saleem, S. Control Volume Finite Element Method for nanofluid MHD natural convective flow inside a sinusoidal annulus under the impact of thermal radiation. *Comput. Methods Appl. Mech. Eng.* **338**, 618–633 (2018).

26. Sheikholeslami, M., Ghasemi, A., Li, Z., Shafee, A. & Saleem, S. Influence of CuO nanoparticles on heat transfer behavior of PCM in solidification process considering radiative source term. *Int. J. Heat Mass Transf.* **126**(A), 1252–1264 (2018).

27. Talavari, A., Ghanavati, B., Azimi, A. & Sayyahi, S. Pvdf/Mwcnt hollow fiber mixed matrix membranes for gas absorption by Al_2O_3 nanofluid. *Prog. Chem. Biochem. Res.* **4**(2), 177–190 (2021).

28. Chand, R., Yadav, D., Bhattacharyya, K. & Awasthi, M. K. Thermal convection in a layer of micropolar nanofluid. *Asia-Pac. J. Chem. Eng* https://doi.org/10.1002/apj.2681 (2021).

29. Alwan, S., Al-Saeed, M. & Abid, H. Safety assessment and biochemical evaluation of biogenic silver nanoparticles (using bark extract of C. zeylanicum) in Rattus norvegicus rats: safety of biofabricated AgNPs (using Cinnamomum zeylanicum extract). *Baghdad J. Biochem. Appl. Biol. Sci.* **2**(3), 138–150 (2021).

30. Taher, M. A., Amine, A. M. & Damarany, B. K. Effect of partial substitution of raw gypsum with thermally treated phosphogypsum on the properties of portland pozzolanic cement. *Adv. J. Chem. A* **2**(4), 296–315 (2019).

31. Chu, Y.-M., Yadav, D., Shafee, A., Li, Z. & Bachf, Q.-V. Influence of wavy enclosure and nanoparticles on heat release rate of PCM considering numerical study. *J. Mol. Liq.* **319**(1), 114121. https://doi.org/10.1016/j.molliq.2020.114121 (2020).

32. Vatnikov, Y. *et al.* Effectiveness of biologically active substances from Hypericum Perforatum L. in the complex treatment of purulent wounds. *Int. J. Pharm. Res.* **9**(3), 74–78 (2017).

33. Beitollahi, H. & Salari, S. Sensitive detection of hydrochlorothiazide using Ce3+/Nio hexagonal nanoparticles modified glassy carbon electrode. *Eurasian chem. commun.* **3**(1), 26–34 (2021).

34. Yi-Peng, X. *et al.* Optimal structure design of a PV/FC HRES using amended Water Strider Algorithm. *Energy Rep.* **7**, 2057–2067 (2021).

35. Abdulameer Salman, F. & Deraman, A. B. Investigating factors affecting the adoption of smartphone technology by elderly people in Iraq. *Rev. Comput. Eng. Res.* **7**(2), 47–53 (2020).

36. Rostamani, M., Hosseinizadeh, S. F., Gorji, M. & Khodadadi, J. M. Numerical study of turbulent forced convection flow of nanofluids in a long horizontal duct considering variable properties. *Int. Commun. Heat Mass Transf.* **37**(10), 1426–1431 (2010).

37. Esmaeilnejad, A., Aminfar, H. & Neistanak, M. S. Numerical investigation of forced convection heat transfer through microchannels with non-Newtonian nanofluids. *Int. J. Therm. Sci.* **75**, 76–86 (2014).

38. Moraveji, M. K., Haddad, S. M. H. & Darabi, M. Modeling of forced convective heat transfer of a non-Newtonian nanofluid in the horizontal tube under constant heat flux with computational fluid dynamics. *Int. Commun. Heat Mass Transf.* **39**(7), 995–999 (2012).

39. Kalteh, M., Abbassi, A., Saffar-Avval, M. & Harting, J. Eulerian–Eulerian two-phase numerical simulation of nanofluid laminar forced convection in a microchannel. *Int. J. Heat Fluid Flow* **32**(1), 107–116 (2011).

40. Mosavi, A., Sedeh, S. N., Toghraie, D. & Karimipour, A. Analysis of entropy generation of ferrofluid flow in the microchannel with twisted porous ribs: The two-phase investigation with various porous layers. *Powder Technol.* **380**, 349–357 (2020).

41. Barnoon, P., Toghraie, D., Eslami, F. & Mehmandoust, B. Entropy generation analysis of different nanofluid flows in the space between two concentric horizontal pipes in the presence of magnetic field: Single-phase and two-phase approaches. *Comput. Math. Appl.* **77**(3), 662–692 (2019).
42. Barnoon, P., Toghraie, D., Dehkordi, R. B. & Abed, H. MHD mixed convection and entropy generation in a lid-driven cavity with rotating cylinders filled by a nanofluid using two phase mixture model. *J. Magn. Magn. Mater.* **483**, 224–248. https://doi.org/10.1016/j.jmmm.2019.03.108 (2019).
43. Alazmi, B. & Vafai, K. Constant wall heat flux boundary conditions in porous media under local thermal non-equilibrium conditions. *Int. J. Heat Mass Transf.* **45**, 3071–3087 (2002).

Author contributions

All authors reviewed the manuscript.

Competing interests

The authors declare no competing interests.

Additional information

Correspondence and requests for materials should be addressed to M.N. or D.T.

Reprints and permissions information is available at www.nature.com/reprints.

Publisher's note Springer Nature remains neutral with regard to jurisdictional claims in published maps and institutional affiliations.